JOURNAL OF COMPUTATIONAL PHYSICS **130,** 217–230 (1997)
ARTICLE NO. CP965579

Kinetic Flux–Vector Splitting for the Navier–Stokes Equations

S. Y. Chou and D. Baganoff

Department of Aeronautics and Astronautics, Stanford University, Stanford, California 94305
E-mail: baganoff@hpsim.stanford.edu

Received October 9, 1995; revised May 28, 1996

Before a hybrid scheme can be developed combining the direct simulation Monte Carlo (DSMC) method and a Navier–Stokes (NS) representation, one must have access to compatible kinetic-split fluxes from the NS portion of the hybrid scheme. The kinetic theory basis is given for the development of the required fluxes from the Chapman–Enskog velocity distribution function for a simple gas; and these are then extended to a polyatomic gas by use of the Eucken approximation. The derived fluxes are then used to implement boundary conditions at solid surfaces that are based on concepts associated with kinetic theory and the DSMC method. This approach is shown to lead to temperature slip and velocity slip as a natural outcome of the new formulation, a requirement for use in the near-continuum regime where DSMC and NS must be joined. Several different flows, for which solid boundaries are not present, are computed using the derived fluxes, together with a second-order finite-volume scheme, and the results are shown to agree well with several established numerical schemes for the NS equations.

I. INTRODUCTION

A question that frequently arises when attempting to model plume flows generated by thrusters operating in the vacuum of space is: how to interface a numerical solution of the Navier–Stokes (NS) equations, which is most appropriate for the high-density gas flow found inside a nozzle, with the direct simulation Monte Carlos (DSMC) method [2], which is most appropriate for modeling the very low-density gas flow found in the outer plume? A similar question arises for the case of a blunt body in a rarefied high-enthalpy flow, where a numerical solution of the NS equations is often the most appropriate for handling the high-density gas layer found near the relatively cold body surface, while the DSMC method is the most appropriate for the rarefied outer flow.

Both questions can best be understood by considering the much simpler case of an impulsively started piston in a stationary gas, where the piston travels in a direction normal to its surface, the piston Mach number is assumed high, and the piston temperature and gas temperature are initially equal. A NS solution for a representative case is shown in Fig. 1, where the piston Mach number is taken to be 5.0 and the gas to be ideal and monatomic. A normal shock wave forms ahead of the piston, the gas temperature (dashed curve) rises behind the shock and then falls as a result of the cold piston surface (located at $x/L = 1$). Because of the nearly constant pressure between the shock and the piston, the density (solid curve) rises in the thermal layer in an inverse ratio to the temperature. In this case, the peak density is 8.2 times the density behind the shock wave. Although the DSMC method must be used to obtain the proper shock wave profile, as is well known, it is clear that the much higher density in the thermal layer would lead to a greatly increased DSMC simulation cost in that region, prompting consideration of a hybrid scheme, where the DSMC method would be used to model the outer flow and the NS equations to model the thermal layer. This concept is schematically depicted in Fig. 2.

Because the DSMC method is based on kinetic theory, the DSMC fluxes to be matched at an interface of a hybrid solution are physical quantities; the fluxes emanating from the DSMC region F^+ are one-sided kinetic fluxes and the frame of reference is an inertial frame, as indicated in Fig. 2. The flux of mass (momentum or energy) from the DSMC side is gotten directly from the particles that cross the interface in one time step. In order to develop an effective hybrid scheme, one must therefore address the following issues.

- The same definitions should be used for the split fluxes when matching at an interface, preferably the kinetic theory definition of one-sided kinetic fluxes (DSMC) in an inertial frame of reference.
- As indicated by Figs. 1 and 2, considerable nonequilibrium may exist at an interface in the form of heat flux or shearing stress when considering a boundary-layer flow. Therefore, the numerical scheme chosen to interface with DSMC must solve the NS equations; because the DSMC method possesses characteristics of a time-dependent finite-volume scheme, compatibility suggests the use of the same scheme for the NS portion.
- Because matching can only be carried out in the near-continuum regime, where both DSMC and NS are valid,

0021-9991/97 $25.00

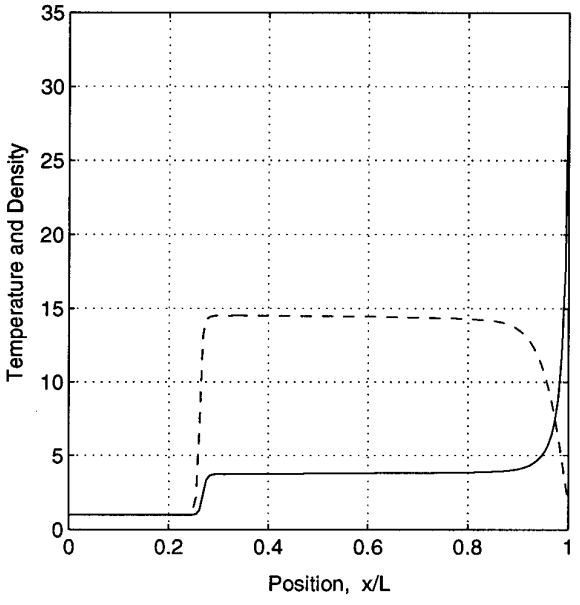

FIG. 1. Temperature (T/T1, – – –) and density ($\rho/\rho 1$, ———) ahead of an impulsively started piston in a stationary gas (state 1), where piston Mach number = 5.0, $\gamma = 5/3$, and piston temperature is held fixed. The piston is located at $x/L = 1$.

it is clear that velocity slip and/or temperature slip would be present at the body surface, i.e., the piston surface in Fig. 2. Therefore, the NS solution must account for slip; the no-slip boundary condition cannot be used.

• The numerical scheme handling the NS portion must be shown to agree with existing numerical methods for the NS equations before a hybrid scheme is constructed.

• Conversion of the NS values for the one-sided kinetic fluxes at an interface into a corresponding collection of particles for insertion into the DSMC simulation must be carried out in a physically compatible and computationally cost-effective way.

• Conditions must be identified that define a suitable location for placement of an interface. For example, for moderate nonequilibrium, it is generally found that good results are obtained for DSMC simulations if the local cell Knudsen number (local mean free path length to cell dimension) is greater than unity. To use this criterion, questions of compatibility with the NS equations would have to be explored.

• Both the NS scheme selected and the resultant hybrid scheme created must be compared with different DSMC solutions for complete verification.

The objective of the present study is to address and discuss the first four issues listed above; the remaining three will be covered in follow-on reports.

Much of the groundwork for the present investigation can be found in a book by Patterson [13] and in papers by Broadwell [4], Bird [2], Pullin [15], Prendergast and Xu [14], Mandal and Deshpande [12], and Gooch [8]. Because we seek a formulation based on the NS equations and because much of the previous work focused on the Euler equations, it is appropriate to first turn to general results found in work on kinetic theory, in particular, the well-known system of moment equations formed from the Boltzmann equation. This approach treats the equilibrium and nonequilibrium components of the fluxes on the same footing, and the derivation itself provides the definitions along with the justification for their use. An alternative is the separate introduction of the nonequilibrium terms at the macroscopic level, as discussed by Macrossan and Oliver [10] and by Mallett *et al.* [11], but this approach would not directly satisfy the first and fifth conditions in the above list of issues.

II. MOMENTS OF THE BOLTZMANN EQUATION

Many of the equations and concepts to be presented in this section can be found in standard work on kinetic theory, such as Chapman and Cowling [5], Grad [9], Patterson [13], Vincenti and Kruger [20], Woods [22], and Bird [3]. We start with the case of an ideal monatomic gas in the absence of external forces and assume the gas is sufficiently dilute for binary collisions to dominate. For this case the Boltzmann equation reads

$$\frac{\partial(nf)}{\partial t} + c_k \frac{\partial(nf)}{\partial x_k} = \left[\frac{\partial(nf)}{\partial t}\right]_{\text{coll}}, \tag{1}$$

where n is the number density, f is the velocity distribution function, c_k the molecular velocity in an inertial frame, the repeated index k denotes a sum, and the right-hand side represents the collision integral. The moment equations are obtained by multiplying the Boltzmann equation by any function of molecular velocity $Q(c_i)$ and integrating over velocity space. These equations are represented by

$$\frac{\partial}{\partial t}(n < Q >) + \frac{\partial}{\partial x_k}(n < c_k Q >) = \Delta[Q]. \tag{2}$$

The two operators appearing in (2) are defined by

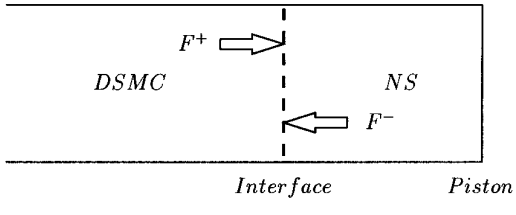

FIG. 2. A schematic representation of a hybrid scheme joining the direct simulation Monte Carlo (DSMC) method and a Navier–Stokes (NS) numerical method.

$$< Q > = \int_{-\infty}^{\infty}\int_{-\infty}^{\infty}\int_{-\infty}^{\infty} Qf dc_1 dc_2 dc_3 \tag{3}$$

and

$$\Delta[Q] = \int_{-\infty}^{\infty}\int_{-\infty}^{\infty}\int_{-\infty}^{\infty} Q\left[\frac{\partial(nf)}{\partial t}\right]_{\text{coll}} dc_1 dc_2 dc_3. \tag{4}$$

When the arbitrary function of molecular velocity $Q(c_i)$ is chosen to be one of the five collisional invariants $Q^{\text{INV}} = m\{1, c_i, c^2/2\}$, where m is the molecular mass and c^2 represents the square of the velocity magnitude, then the corresponding moment of the collision integral is identically zero, i.e., $\Delta[Q^{\text{INV}}] = 0$. This is a general result that holds for any distribution function f and for any molecular interaction law. This selection leads to the conservation laws for gas dynamics, which can be written in the form

$$\frac{\partial}{\partial t}(n < Q^{\text{INV}} >) + \frac{\partial}{\partial x_k}(n < c_k Q^{\text{INV}} >) = 0, \tag{5}$$

or, when using each of the collisional invariants in turn, one obtains the set

$$\frac{\partial}{\partial t}(\rho) + \frac{\partial}{\partial x_k}(\rho \langle c_k \rangle) = 0 \tag{6a}$$

$$\frac{\partial}{\partial t}(\rho < c_i >) + \frac{\partial}{\partial x_k}(\rho \langle c_k c_i \rangle) = 0 \tag{6b}$$

$$\frac{\partial}{\partial t}(\rho < c^2/2 >) + \frac{\partial}{\partial x_k}(\rho < c_k c^2/2 >) = 0, \tag{6c}$$

where $\rho = mn$ is the mass density.

Introduction of the thermal velocity components $C_i = (c_i - u_i)$, where $u_i = < c_i >$ is the mean or fluid velocity, allows one to introduce the central moments defined by

$$P_{ij} = \rho < C_i C_j > \tag{7}$$

$$p = P_{kk}/3 \tag{8}$$

$$\tau_{ij} = -P_{ij} + p\delta_{ij} \tag{9}$$

$$e = < C^2/2 > \tag{10}$$

$$q_i = \rho < C_i C^2/2 >, \tag{11}$$

where P_{ij} is the pressure tensor or stress tensor, p is the pressure, τ_{ij} is the viscous stress tensor, e is the internal energy (translational) for a monatomic gas, and q_i is the heat flux vector for a monatomic gas. The conservation laws for gas dynamics can then be written in the familiar form

$$\frac{\partial}{\partial t}(\rho) + \frac{\partial}{\partial x_k}(\rho u_k) = 0 \tag{12a}$$

$$\frac{\partial}{\partial t}(\rho u_i) + \frac{\partial}{\partial x_k}(\rho u_k u_i + P_{ki}) = 0 \tag{12b}$$

$$\frac{\partial}{\partial t}\left[\rho\left(e + \frac{u^2}{2}\right)\right] + \frac{\partial}{\partial x_k}\left[\rho u_k\left(e + \frac{u^2}{2}\right) + P_{ki}u_i + q_k\right] = 0. \tag{12c}$$

If the gas is not simply a monatomic gas but has internal structure, then the above procedure must be modified. Because the general problem includes the question of what equation replaces (1), the problem is rather difficult and it becomes necessary to make use of a suitable approximation. One simplistic approach is to assume that all internal molecular energy modes are in equilibrium, both internally and with the translational degrees of freedom. Thus, the additional internal energy e_{int} can be expressed in terms of the translational temperature T by the equilibrium relation

$$e_{\text{int}} = \frac{1}{2}\left(\frac{5 - 3\gamma}{\gamma - 1}\right) RT, \tag{13}$$

where R is the gas constant and where an accounting for the additional internal energy is introduced through the ratio of specific heats γ and for which $e_{\text{int}} = 0$ in the case of a monatomic gas.

To properly account for the amount of energy that is carried by a particle with internal structure, the energy $mc^2/2$ must be replaced by $(mc^2/2 + \varepsilon)$, where ε is the additional internal energy per particle, and therefore, the quantities of interest become

$$Q^{\text{INV}} = \{m, mc_i, (mc^2/2 + \varepsilon)\}. \tag{14}$$

Assuming Eq. (1) continues to hold for the extended distribution function $f(c_i, \varepsilon)$ and provided the right-hand side is interpreted in a suitable way, then an additional integral over ε is formally required in applying both (3) and (4). It is reasonable to argue, however, that the quantities in (14) must continue to be conserved in a collision, and consequently, (4) again evaluates to zero; thus, (5) remains unchanged.

In evaluating the left-hand side of (5) for the five different quantities in (14), identical results to those obtained for the monatomic gas will be found for all quantities that contain polynomials in c_i alone. This follows from the fact that integration over the ε variable can be taken first and independently from the c_i integration. Therefore, Eqs. (6a) and (6b) and, consequently, (12a) and (12b), are fully recovered. The same conclusion also applies to the first term

in the quantity $(mc^2/2 + \varepsilon)$ and, therefore, (6c) is replaced by

$$\frac{\partial}{\partial t}(\rho < c^2/2 > + n < \varepsilon >) + \frac{\partial}{\partial x_k}(\rho < c_k c^2/2 > + n < c_k \varepsilon >) = 0. \tag{15}$$

Substitution of the central moments (7)–(11) into (15) reproduces all of the previous algebra for the monatomic gas and leads to

$$\frac{\partial}{\partial t}\left[\rho\left(e + \frac{u^2}{2}\right) + \rho e_{\text{int}}\right] + \frac{\partial}{\partial x_k}\left[\rho u_k\left(e + \frac{u^2}{2}\right) + P_{ki}u_i + q_k + (n < C_k \varepsilon > + \rho u_k e_{\text{int}})\right] = 0, \tag{16}$$

where the definition $< \varepsilon > = m e_{\text{int}}$ has been used. Therefore (12c) also continues to hold, provided we replace (10) by

$$e = (< C^2/2 > + e_{\text{int}}) \tag{17}$$

and the definition of the heat flux vector (11) by

$$q_i = \rho < C_i C^2/2 > + n < C_i \varepsilon >. \tag{18}$$

We therefore conclude that the complete collection of Eqs. (5), (6), and (12) can be used as they stand, provided definitions (17) and (18) are employed when the gas possesses internal structure and a state of equilibrium exists between the internal modes and the translational degrees of freedom (see [20, p. 326]).

Because the conservation equations (12) can be developed for any general fluid through use of phenomenological arguments alone, the set is actually more general than the kinetic theory derivation would indicate, i.e., they are also the conservation equations for fluid dynamics. However, we are only interested in treating an ideal gas flow, and the use of the kinetic theory approach is necessary because it shows that the set is valid for any degree of translational nonequilibrium, that is, for any translational velocity distribution function one cares to consider. If one chooses the equilibrium distribution, namely the Maxwellian distribution f^{Max}, then the set becomes the Euler equations, because viscous stress and heat flux are identically zero for f^{Max}. This step allows one, in effect, to reproduce the special case considered by Pullin [15] in his equilibrium flux method (EFM), as well as the work by Mandal and Deshpande [12] on kinetic flux-vector splitting (KFVS) for the Euler equations. The inviscid limit of the recent work by Mallett *et al.* [11] is also recovered by this step. If one chooses a Chapman–Enskog (CE) distribution f^{CE}, then the set becomes the Navier–Stokes equations, because stress and heat flux are then given by the corresponding Chapman–Enskog expressions. This is the path that we will follow in developing a KFVS scheme for the NS equations. One may also choose a discrete representation for f and the equations still hold. This is an alternate interpretation of the concept that lies behind the state vector splitting scheme for the Navier–Stokes equations introduced by Gooch [8]. The most important point is that one is free to choose any translational velocity distribution function whatsoever in using Eqs. (5), (6), or (12), and in so doing, the set becomes closed, as long as f is fully specified. Otherwise, if f remains general, then one is faced with the well-known closure problem, when using a moment method, because τ_{ij} and q_i are then unknown quantities in the equations. It is useful to emphasize the fact that the conservation equations as displayed in (12) are not the NS equations until one introduces f^{CE}.

Each of the five separate moment equations represented by either (5), (6), or (12) can be expressed by the single form

$$\frac{\partial U}{\partial t} + \frac{\partial F_k}{\partial x_k} = 0. \tag{19}$$

The complete specification of F_i in three dimensions, as defined by (19), requires the evaluation of 15 quantities. But the task is made considerably simpler, if one considers a finite volume scheme, uses Gauss' divergence theorem, and writes Eq. (19) as

$$\frac{\partial}{\partial t}\int_V U\, dV + \int_S F_n\, dS = 0, \tag{20}$$

where S encloses the volume V and F_n is the projection of F_i onto the unit outward pointing normal for the surface element dS. If V is taken to be a rectangular volume, then one only needs to evaluate five quantities for each planar surface, a conceptually simpler task, provided F_n can be evaluated directly. Using the notation of (5), we then have

$$U = n < Q^{\text{INV}} > \tag{21}$$

and

$$F_n = n < c_n Q^{\text{INV}} >, \tag{22}$$

where U is the state vector, F_n is the total flux vector, and c_n is the component of the molecular velocity normal to the planar surface. Equation (22) clearly represents a physical concept. This can be seen from the fact that Q is a scalar

quantity which is carried across the fixed surface by c_n, thus creating a physical flux in that quantity.

The five fluxes defined by (22) are total fluxes, not the one-sided fluxes depicted in Fig. 2. In addition, these general expressions contain both the inviscid fluxes as well as the nonequilibrium components due to viscous stress and heat flux, as can be seen from the corresponding terms in (12). Because many quantities evaluate to zero in arriving at the set (12) and these cannot be recovered in a simple way, one must use the more primitive set (5), or (6), in developing the algebra for the one-sided, kinetic-split fluxes.

III. KINETIC SPLIT FLUXES

As seen in Fig. 2, we are interested in expressions for the one-sided fluxes based on a fixed interface and an inertial frame of reference. On this basis and on considering the x_1 direction as positive, we can split the integration in c_1 as

$$\begin{aligned}\int_{-\infty}^{\infty}\int_{-\infty}^{\infty}\int_{-\infty}^{\infty}\{....\}\,dc_1dc_2dc_3 &= \int_{-\infty}^{\infty}\int_{-\infty}^{\infty}\left(\int_{-\infty}^{0}+\int_{0}^{\infty}\right)\{....\}\,dc_1dc_2dc_3 \\ &= \int_{-\infty}^{\infty}\int_{-\infty}^{\infty}\left(\int_{-\infty}^{-u_1}+\int_{-u_1}^{\infty}\right)\{...\}\,dC_1dC_2dC_3,\end{aligned} \tag{23}$$

where the second expression introduces the thermal velocity components C_i. The concept of a kinetic split flux has a long history in kinetic theory and a clear application to an equilibrium flow can be found in a textbook by Patterson (Ref. [13, pp. 163–167]). On using the notation to represent the splitting in (23)

$$F = F^- + F^+ \tag{24}$$

and on introducing a Cartesian coordinate system (n, $t1$, $t2$), located in an arbitrary fixed planar surface, we obtain from (22), (23), and (24) the definitions

$$F_n^- = n\int_{-\infty}^{\infty}\int_{-\infty}^{\infty}\int_{-\infty}^{-u_n}(C_n+u_n)Q^{\mathrm{INV}}f\,dC_ndC_{t1}dC_{t2} \tag{25}$$

$$F_n^+ = n\int_{-\infty}^{\infty}\int_{-\infty}^{\infty}\int_{-u_n}^{\infty}(C_n+u_n)Q^{\mathrm{INV}}f\,dC_ndC_{t1}dC_{t2}. \tag{26}$$

These relations provide the means for computing F_n when f is a known function.

Because the total fluxes are known from the terms in (12), explict expressions for each of the collisional invariants given by (14) need only be listed for, say, F_n^+. It is also useful to introduce a more physically descriptive notation for the split fluxes as follows:

$$F^+_{\mathrm{zero}} = \int_{-\infty}^{\infty}\int_{-\infty}^{\infty}\int_{-u_n}^{\infty}f\,dC_ndC_{t1}dC_{t2} \tag{27}$$

$$F^+_{\mathrm{mass}} = \rho\int_{-\infty}^{\infty}\int_{-\infty}^{\infty}\int_{-u_n}^{\infty}(C_n+u_n)f\,dC_ndC_{t1}dC_{t2} \tag{28}$$

$$F^+_{n\text{-mom}} = \rho\int_{-\infty}^{\infty}\int_{-\infty}^{\infty}\int_{-u_n}^{\infty}(C_n+u_n)^2f\,dC_ndC_{t1}dC_{t2} \tag{29}$$

$$F^+_{t1\text{-mom}} = \rho\int_{-\infty}^{\infty}\int_{-\infty}^{\infty}\int_{-u_n}^{\infty}(C_n+u_n)(C_{t1}+u_{t1})\,f\,dC_ndC_{t1}dC_{t2} \tag{30}$$

$$F^+_{\mathrm{tr-energy}} = \rho\int_{-\infty}^{\infty}\int_{-\infty}^{\infty}\int_{-u_n}^{\infty}(C_n+u_n)\,[(C_n+u_n)^2+(C_{t1}+u_{t1})^2+(C_{t2}+u_{t2})^2]\,\frac{1}{2}f\,dC_ndC_{t1}dC_{t2} \tag{31}$$

$$F^+_{\mathrm{int-energy}} = n\int_0^{\infty}\int_{-\infty}^{\infty}\int_{-\infty}^{\infty}\int_{-u_n}^{\infty}(C_n+u_n)\,\varepsilon f\,dC_ndC_{t1}dC_{t2}\,d\varepsilon = \Delta q^+_{\mathrm{Eucken}} + \rho u_n e^+_{\mathrm{int}} \tag{32}$$

$$F^+_{\mathrm{energy}} = F^+_{\mathrm{tr-energy}} + F^+_{\mathrm{int-energy}}. \tag{33}$$

Integration over the ε variable is not shown in Eqs. (27)–(31) because it can be carried out as an independent operation and done first. However, it does appear explicitly in (32), and this equation must be included when a gas has internal structure. The role played by (32) can be seen from the fact that the $C_n\varepsilon$ term in the integrand is the source of the second term in (18), while the $u_n\varepsilon$ term is the source of the second term in (17). The difficulty in applying (32) results from the fact that we need an explicit expression for the joint distribution $f(C_i, \varepsilon)$ in order to evaluate these split fluxes; and this lack of knowledge is indicated by the notation employed following the second equality. However, in the case of the total e_{int}, it is given by (13) since our model assumes equilibrium for the internal degrees of freedom. Likewise, for the total flux represented by $\Delta q_{\mathrm{Eucken}}$, we can use the Eucken model which replaces $< C_n\varepsilon >$ by a quantity that is proportional to the temperature gradient, thus making it proportional to the heat flux vector (see [22, p. 66]). The net effect changes the value of the coefficient of thermal conductivity, as well as the Prandtl number, from that for a simple gas to the proper values for a gas with internal structure. This then allows one to use the same basic relations found for a simple gas. We will use the Eucken approximation and represent the incremental contribution to the heat flux due to the internal degrees of freedom by

$$\Delta q_{\mathrm{Eucken}} = \Delta q^-_{\mathrm{Eucken}} + \Delta q^+_{\mathrm{Eucken}} = -K''\nabla T. \tag{34}$$

These steps alone, however, still do not answer the ques-

tion of how one evaluates the split fluxes appearing in (32). This will be done after we have completed the implementation of the Eucken model.

The extra quantity F^{+}_{zero} is also listed because it defines how the velocity distribution function itself is split, which is needed in the overall algebra. This can be seen from the normalization condition $F_{\text{zero}} = F^{-}_{\text{zero}} + F^{+}_{\text{zero}} = 1$ for a probability distribution. The expression for $F^{+}_{t2-\text{mom}}$ is not listed because it can be gotten by merely interchanging $t1$ and $t2$ in (30). For a monatomic gas, the set of equations is very general and applies for any velocity distribution function one cares to define, for example, even for a discrete distribution. For a polyatomic gas, the set is not quite as general and is limited by the Eucken model and the approximations to be introduced below. Our interest is in the Chapmann–Enskog distribution and the resulting split fluxes.

IV. CHAPMAN–ENSKOG SPLIT FLUXES

A gas flow that is in thermodynamic equilibrium is represented locally by a Maxwellian distribution, and a gas flow that is slightly disturbed from the equilibrium state is represented locally by the Chapman–Enskog (CE) distribution. The CE distribution is obtained as an approximate solution of the Boltzmann equation (for a simple gas) and is expressed as a product of a local Maxwellian and a polynomial function of the thermal velocity components C_i, that is, by the relation

$$f^{\text{CE}} = f^{\text{Max}}\,(1 + \phi_1 + \phi_2) \tag{35}$$

where

$$f^{\text{Max}} = (2\pi RT)^{-3/2}\exp(-C^2/2RT)$$

$$\phi_1 = -\left(\frac{\rho}{p^2}\right)\left(K^{(1)}\frac{\partial T}{\partial x_k}\right)C_k\,(C^2/5RT - 1)$$

$$\phi_2 = -\left(\frac{\rho}{p^2}\right)\left(\mu^{(1)}\frac{\partial u_j}{\partial x_k}\right)\left(C_jC_k - \frac{1}{3}C^2\delta_{jk}\right),$$

and where $K^{(1)}$ is the coefficient of thermal conductivity and $\mu^{(1)}$ is the coefficient of viscosity as determined by the first-order Chapmann–Enskog procedure, and δ_{jk} is the Kronecker delta. Because both the temperature gradient and the velocity-gradient tensor appear as parameters in f^{CE}, notational efficiency can be gained in the algebra that follows by replacing those quantities by the Chapman–Enskog expressions for stress and heat flux, i.e., by

$$q_i^{\text{CE}} = -K^{(1)}\frac{\partial T}{\partial x_i} \tag{36}$$

$$\tau_{ij}^{\text{CE}} = \mu^{(1)}\left(\frac{\partial u_i}{\partial x_j} + \frac{\partial u_j}{\partial x_i}\right) - \frac{2}{3}\mu^{(1)}\left(\frac{\partial u_k}{\partial x_k}\right)\delta_{ij}. \tag{37}$$

At this point we face a logical difficulty. Must we fix the Prandtl number to the value for a simple gas ($\text{Pr} = \mu^{(1)} c_p/K^{(1)} = 2/3$) or may we allow it to vary so that (36) becomes consistant with the Eucken approximation? As there is no simple answer, we will defer the question to the point in the analysis where logical conflicts can be more easily identified. On substituting (35) into Eqs. (27)–(31) and using the same orthogonal coordinate system (n, $t1$, $t2$), we see that in each case the integrand becomes a product of polynomials in the thermal velocities C_i and the Maxwellian distribution f^{Max}. The only difficulty that appears in carrying out the integration is the large number of terms that are produced. For example, ϕ_1 and ϕ_2 are composed of four and nine terms, respectively, and therefore (35) leads to a total of 14 terms. On evaluating $F^{+}_{\text{tr-energy}}$ alone, we are faced with 252 terms. This at first appears to be an overwhelming task, until it is noticed that many of the terms are zero, because in the C_{t1} and C_{t2} variables all odd moments of the symmetric function f^{Max} are zero and even moments are well-known functions of RT. Likewise, integration in the C_n component can be handled by splitting the integration into $-u_\infty$ to $0 + 0$ to ∞ which then leads to exponential and error functions (see [3, p. 417]). Because the collection of functions is small, there is hope that the results can be finally assembled into fairly compact expressions. Even though the details are daunting, Patterson (Ref. [13, p. 77]) used a method he reports was ''initiated by Maxwell and developed by Chapman'' to develop general expressions for the total fluxes, for the case of nonisentropic flow, which employs concepts and algebra very similar to that employed here. Our interest, however, is in obtaining the split fluxes for which many more terms must be handled. To carry out the present study, intensive use of symbolic mathematical manipulations, provided by MATHEMATICA, was made in handling the algebra. Only the final collected integrated results wil be presented here. A discussion of the detailed steps required to obtain the following relations can be found in [6]:

$$F^{\pm}_{\text{zero}} = \tfrac{1}{2}[(1 \pm \alpha_1) \pm \alpha_2\,(S_n\hat{\tau}^{\text{CE}}_{nn} + (2S_n^2 - 1)\hat{q}^{\text{CE}}_n)] \tag{38}$$

$$F^{\pm}_{\text{mass}} = \rho\sqrt{RT/2}\,[(1 \pm \alpha_1)S_n \pm \alpha_2\,(1 - \chi_1)] \tag{39}$$

$$F^{\pm}_{n-\text{mom}} = p\,[(1 \pm \alpha_1)(S_n^2 + \tfrac{1}{2}(1 - \hat{\tau}^{\text{CE}}_{nn})) \pm \alpha_2\,(S_n + \hat{q}^{\text{CE}}_n)] \tag{40}$$

$$F^{\pm}_{t1-\text{mom}} = \sqrt{2RT}\,[S_{t1}F^{\pm}_{\text{mass}}] + \tfrac{1}{2}p\,[-(1 \pm \alpha_1)\tau^{\wedge\text{CE}}_{nt1} \pm \alpha_2\hat{q}^{\text{CE}}_{t1}] \tag{41}$$

$$F^{\pm}_{\text{tr-energy}} = p\sqrt{RT/2}\,[(1 \pm \alpha_1)(S_n(\tfrac{5}{2} + S^2) + \chi_2) \pm \alpha_2(2 + S^2 + \chi_3)] \tag{42}$$

$$F^{\pm}_{\text{int-energy}} = (\Delta q^{\pm}_{\text{Eucken}} + \rho u_n e^{\pm}_{\text{int}}) = \frac{1}{2}\left(\frac{5-3\gamma}{\gamma-1}\right)[RT\,F^{\pm}_{\text{mass}}] \tag{43}$$

$$F^{\pm}_{\text{energy}} = F^{\pm}_{\text{tr-energy}} + F^{\pm}_{\text{int-energy}}, \tag{44}$$

where

$$\alpha_1 = \text{er f}(S_n), \quad \alpha_2 = \frac{1}{\sqrt{\pi}}e^{-S_n^2}$$

$$\chi_1 = \left[S_n\hat{q}_n^{\text{CE}} + \frac{1}{2}\hat{\tau}_{nn}^{\text{CE}}\right]$$

$$\chi_2 = \left[\frac{5}{2}\hat{q}_n^{\text{CE}} - (S_n\hat{\tau}_{nn}^{\text{CE}} + S_{t1}\hat{\tau}_{nt1}^{\text{CE}} + S_{t2}\hat{\tau}_{nt2}^{\text{CE}})\right]$$

$$\chi_3 = [S_{t1}\hat{q}_{t1}^{\text{CE}} + S_{t2}\hat{q}_{t2}^{\text{CE}} - \chi_1(1 + S_{t1}^2 + S_{t2}^2) - \hat{\tau}_{nn}^{\text{CE}}]$$

$$S_n = u_n/\sqrt{2RT}, \quad S^2 = S_n^2 + S_{t1}^2 + S_{t2}^2$$

$$\hat{\tau}_{nn}^{\text{CE}} = \tau_{nn}^{\text{CE}}/p, \qquad \hat{q}_n^{\text{CE}} = \frac{2}{5}q_n^{\text{CE}}/(p\sqrt{2RT}).$$

Each individual component of S_i, $\hat{\tau}_{ij}$, and $\hat{q}_i$ is not listed, as they are clearly nondimensionalized the same way.

Equations (38)–(42) are not outwardly affected by the physics associated with additional internal degrees of freedom, i.e., $\gamma \neq \frac{5}{3}$. In view of this, these equations should not contain γ explicitly, when expressed appropriately. This is easily done by introducing the speed ratio $S = u/\sqrt{2RT}$, which is frequently used in kinetic theory, as opposed to the Mach number, which requires the introduction of γ through the isentropic speed of sound. Use of the speed ratio S not only provides a useful physical check on the mathematical results, it also allows the final expressions to be written in a more compact form. On the other hand, the physical concepts that lead to (43) directly involve additional internal degrees of freedom and the relation should contain γ explicitly, which is seen in the expression that follows the second equality, a step to be explained in the following discussion.

It is appropriate to review several consistency checks on Eqs. (38)–(43). First, the total fluxes (24) should agree with the corresponding expressions in (12). Starting with (38), we have $F_{\text{zero}} = 1$, which is the correct normalization condition for a proability distribution. From (39)–(43), we have

$$F_{\text{mass}} = \rho u_n \tag{45}$$

$$F_{n\text{-mom}} = \rho u_n^2 + p - \tau_{nn}^{\text{CE}} \tag{46}$$

$$F_{t1\text{-mom}} = \rho u_n u_{t1} - \tau_{nt1}^{\text{CE}} \tag{47}$$

$$F_{\text{tr-energy}} = \rho u_n\left(\frac{3}{2}RT + \frac{u^2}{2}\right) + pu_n - (\tau_{nn}^{\text{CE}}u_n + \tau_{nt1}^{\text{CE}}u_{n1} + \tau_{nt2}^{\text{CE}}u_{t2}) + q_n^{\text{CE}} \tag{48}$$

$$F_{\text{int-energy}} = (\Delta q_{\text{Eucken}} + \rho u_n e_{int}) = \frac{1}{2}\left(\frac{5-3\gamma}{\gamma-1}\right)pu_n. \tag{49}$$

These correspond to all the expressions in (12) for the orthogonal coordinated system used. Equation (49) provides both the extra term required by (17), as well as the extra term required by (18). However, this returns us to the logical difficulty raised in the discussion following (36) and (37). If the Eucken approximation is introduced when first using (36), then its effect will appear twice when summing (48) and (49), i.e., in the combination $(q_n^{\text{CE}} + \Delta q_{\text{Eucken}})$. Knowing this, one approach would be to introduce the Eucken approximation here by absorbing Δq_{Eucken} into the term q_n^{CE} by using Eq. (34). Although it appears to be a reasonable step, it is in fact a bold step, because split fluxes are required in (42) and (43) and one cannot be sure that when the Eucken approximation is introduced into χ_2 and χ_3 in (42) that it will properly account for the absorption of the split quantities $\Delta q^{\pm}_{\text{Eucken}}$ in (43). Consequently, one may encounter incorrect energy split fluxes at an interface or a boundary. Actually, we have no alternative, as we do not have $f(C_i, \varepsilon)$ with which to compute these split quantities. In the following development, we will use the Eucken approximation throughout and assume that proper accounting is made for $\Delta q^{\pm}_{\text{Eucken}}$ by χ_2 and χ_3.

An additional assumption is actually needed to complete the specification of (43), and this involves the evaluation of $e^{\pm}_{\text{int}}$, which again requires knowledge of $f(C_i, \varepsilon)$. Assuming the Eucken model properly accounts for the correlation $\Delta q_{\text{Eucken}} = n < C_n\varepsilon >$ then it may be permissible to employ the equilibrium assumption to approximate $e^{\pm}_{\text{int}}$. The assumption that the internal energy modes are in equilibrium, both internally and with the translational degrees of freedom, leads to the conclusion that C_i and ε are statistically independent random variables, and therefore, $f(C_i, \varepsilon)$ reduces to a product function. On this basis $e^{\pm}_{\text{int}}$ can be evaluated, and this step leads to the expression following the second equality in (43). However, we should note that if the same assumption were used to evaluate $< C_n\varepsilon >$ as well, then we would have $\Delta q_{\text{Eucken}} = n < C_n\varepsilon > = n < C_n >< \varepsilon > = 0$ because $< C_n > = 0$ by definition; and this would lead to the loss of the Eucken approximation. In summary, on combining (42) and (43), our approach consists of absorbing $\Delta q^{\pm}_{\text{Eucken}}$ into χ_2 and χ_3 by the introduction of the Eucken approximation and using the equilibrium

assumption to evaluate $e^{\pm}_{\text{int}}$; this leads to the second expression in (43) as well as the second expression in (49).

A second check leads to the requirement that one should recover the known values for the Maxwellian distribution when setting the nonequilibrium parameters $\hat{\tau}^{\text{CE}}$ and $\hat{q}^{\text{CE}}$ to zero:

$$F^{\pm}_{\text{zero}} = \tfrac{1}{2}(1 \pm \alpha_1) \tag{50}$$

$$F^{\pm}_{\text{mass}} = \rho\sqrt{RT/2}\,[(1 \pm \alpha_1)S_n \pm \alpha_2] \tag{51}$$

$$F^{\pm}_{n\text{-mom}} = p\,[(1 \pm \alpha_1)(S_n^2 + \tfrac{1}{2}) \pm \alpha_2 S_n] \tag{52}$$

$$F^{\pm}_{t1\text{-mom}} = \sqrt{2RT}\,[S_{t1} F^{\pm}_{\text{mass}}] \tag{53}$$

$$F^{\pm}_{\text{tr-energy}} = p\sqrt{RT/2}\,[(1 \pm \alpha_1)S_n(\tfrac{5}{2} + S^2) \pm \alpha_2(2 + S^2)] \tag{54}$$

$$F^{\pm}_{\text{int-energy}} = \frac{1}{2}\left(\frac{5 - 3\gamma}{\gamma - 1}\right)[RT\,F^{\pm}_{\text{mass}}]. \tag{55}$$

These expressions are in full agreement with results obtained by Patterson (Ref. [13, Section 5.3, Eqs. (4), (11), (17), (19)]), where his objective was to compute the momentum and energy exchange at a surface for an equilibrium gas. These relations were later introduced in work by Pullin [15] (for one-dimensional flow) and more recently by Mandal and Deshpande [12] and by Mallett *et al.* [11].

Finally, on setting the fluid velocities to zero ($S = 0$, $\alpha_1 = 0$, $\alpha_2 = 1/\sqrt{\pi}$), one must recover the well-known kinetic theory values for a stationary equilibrium distribution (Maxwellian):

$$F^{\pm}_{\text{zero}} = 1/2 \tag{56}$$

$$F^{\pm}_{\text{mass}} = \pm\,\rho\sqrt{RT/2\pi} \tag{57}$$

$$F^{\pm}_{n\text{-mom}} = p/2 \tag{58}$$

$$F^{\pm}_{t1\text{-mom}} = 0 \tag{59}$$

$$F^{\pm}_{\text{tr-energy}} = \pm\,p\sqrt{2RT/\pi} \tag{60}$$

$$F^{\pm}_{\text{int-energy}} = \pm\frac{1}{2}\left(\frac{5 - 3\gamma}{\gamma - 1}\right)p\sqrt{RT/2\pi}. \tag{61}$$

The first five relations clearly agree with known values in kinetic theory, while the final relation is based on several critical assumptions as discussed above.

The importance of the nonequilibrium parameters $\hat{\tau}^{\text{CE}}_{ik}$ and $\hat{q}^{\text{CE}}_{k}$ in Eqs. (39)–(44) can be judged by comparison with equivalent Euler split fluxes. Of interest in a comparison are the Steger–Warming split fluxes [17] and the equilibrium values given by (51)–(55). Obviously, the nonequilibrium parameters are not constants in a flow, but in a graphical display representative values are quite useful, and a representative peak value for both parameters in a moderately strong normal shock wave is roughly -0.3. This value, along with $\gamma = 1.4$ and the assumption of a one-dimensional flow, was used to develop Fig. 3, which presents the momentum and energy split fluxes versus the local Mach number for three cases: KFVS for the NS equations given by (40) and (44); KFVS for the Euler equations given by (52) and the sum of (54) and (55); and Steger–Warming splitting. On the scale shown, the results for the equilibrium values and Steger–Warming group fairly closely together (a comparison apparently first made by Mandal and Deshpande [12]), while the present work shows considerable difference, especially in the asymmetrical shift seen in F^+ and F^-. The figure clearly points to the fact that in a hybrid solution, where the one-sided fluxes are to be matched at an interface having nonequilibrium conditions, the present kinetic split fluxes must be used. This is because one does not otherwise know how to adjust the Euler split fluxes to account for viscous and heat conduction effects, even though the total fluxes are known from (12).

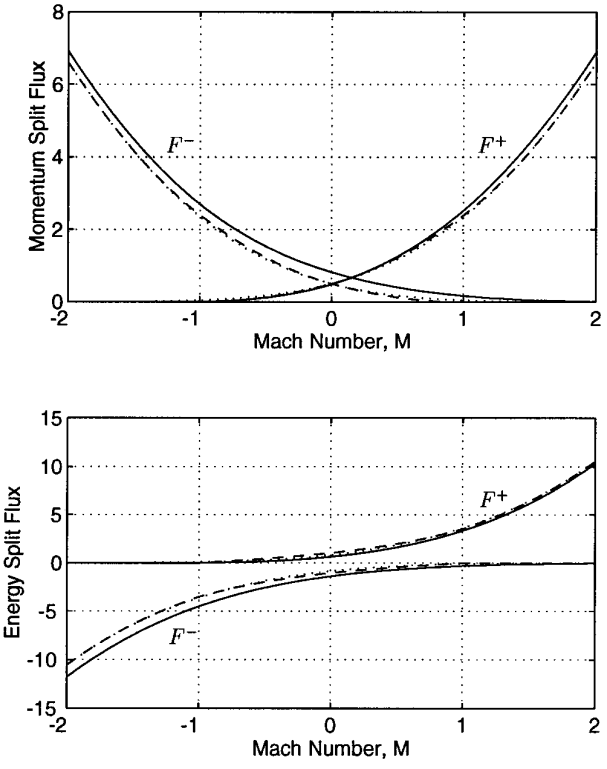

FIG. 3. Momentum and energy split fluxes for the case of a one-dimensional flow and $\gamma = 1.4$. The momentum flux is nondimensionalized by p and the energy flux by $p(2RT)^{1/2}$. Comparisons are for the present work, where the assumption $\hat{\tau}^{\text{CE}}_{nn} = \hat{q}^{\text{CE}}_{n} = -0.3$ was made in Eqs. (40) and (44), ———; Mandal–Deshpande KFVS for the Euler equations, · · ·; and Steger-Warming, – – –.

V. BOUNDARY CONDITIONS

When a nonreacting particle in the DSMC method passes through a body surface during a time step, the procedure is to emit the same particle from the surface with a new velocity depending on the boundary conditions. Thus, the DSMC method effectively treats a solid boundary as though it too consists of a gas, but at different conditions. This concept was clearly described by Patterson (Ref. [13, p. 165]) and was used in his analysis of molecular interactions with boundaries. Because the same particle is emitted, the wall gas is identically the same gas and, therefore, the two share the same molecular mass and gas constant. Also, because every particle passing through a body surface is treated this way, the number of particles per unit time per unit area passing into a wall is exactly balanced by the rate of emission. However, this condition does not tell us what the number density of the wall gas is; i.e., it does not fix n_w, or ρ_w, for the wall gas, nor does it fix the temperature of the wall gas T_w. What we do know is that the total mass flux must be zero at a material surface, i.e.,

$$(F_{\text{mass}})_{\text{surface}} = (F^{+}_{\text{mass}})_g + (F^{-}_{\text{mass}})_w = 0, \tag{62}$$

where gas and wall positions, consistent with the end-wall geometry shown in Fig. 2, are assumed. Generally speaking, in the DSMC method one often assumes that the wall gas is in equilibrium and the wall is stationary. On this basis, Eq. (57) can be used in (62) to describe the wall gas, and we can write

$$(F^{+}_{\text{mass}})_g = \rho_w \sqrt{RT_w/2\pi}. \tag{63}$$

A particularly simple boundary condition is the case where the wall temperature T_w is specified, namely, an isothermal boundary condition; for this case Eq. (63) fixes the density of the wall gas ρ_w, since $(F^{+}_{\text{mass}})_g$ would be known from (39) and the state of the gas from the update procedure for the numerical solution of the NS equations. Given ρ_w, T_w and $p_w = \rho_w R T_w$, we then have, on using (58), the relation

$$(F_{n-\text{mom}})_{\text{surface}} = (F^{+}_{n-\text{mom}})_g + p_w/2, \tag{64}$$

which fixes the normal stress at the surface, since $(F^{+}_{n-\text{mom}})_g$ likewise represents a known quantity from (40) and the update procedure. Likewise, on using (59), we have

$$(F_{t1-\text{mom}})_{\text{surface}} = (F^{+}_{t1-\text{mom}})_g, \tag{65}$$

which determines the tangential stress on the surface. Finally, the energy flux to the surfaces is found by using (60) and (61), together with (44) and the state of the gas from the update procedure; i.e.,

$$(F_{\text{energy}})_{\text{surface}} = (F^{+}_{\text{energy}})_g - p_w \sqrt{2RT_w/\pi}\left[1 + \frac{1}{4}\left(\frac{5-3\gamma}{\gamma-1}\right)\right], \tag{66}$$

which completes the specification of the conditions at a surface for an isothermal wall. The most important outcome from this analysis is that the temperature of the gas near the surface may not be equal to the specified wall temperature T_w, which gives rise to the possibility of temperature slip. Likewise, the tangential velocity near the surface may not be zero, leading to velocity slip; however, the normal velocity near the surface must be zero because the expressions in (62) also define the fluid velocities for the two separate gases.

For an adiabatic boundary condition, we know that the total energy flux to the surface is zero, while the wall gas temperature and density are unknown. Thus, we have

$$(F_{\text{energy}})_{\text{surface}} = (F^{+}_{\text{energy}})_g + (F^{-}_{\text{energy}})_w = 0. \tag{67}$$

On using (60) and (61) for the wall gas, we have

$$(F^{+}_{\text{energy}})_g = p_w \sqrt{2RT_w/\pi}\left[1 + \frac{1}{4}\left(\frac{5-3\gamma}{\gamma-1}\right)\right], \tag{68}$$

which along with (63) provides two equations in the two unknowns ρ_w and T_w, since $(F^{+}_{\text{mass}})_g$ and $(F^{+}_{\text{energy}})_g$ are both known from the update procedure at each time step. Likewise, the normal stress on the surface can be obtained using (58) and the tangential stress using (59), completing the analysis.

The application of flux boundary conditions to the wide variety of possible boundary conditions is quite straightforward and only two are given here. For example, accommodation coefficients for momentum and energy are often used in the application of the DSMC method, and it would be a simple matter to include them as well. In addition, analytical results for both temperature slip and velocity slip can be obtained from Eqs. (62)–(68) and these can be shown to reproduce the special case considered by Patterson (Ref. [13, Section 4.4, Eqs. (30)–(33)]). A detailed discussion of this topic will be covered in a follow-on report.

VI. NUMERICAL COMPARISONS

Our main objective is to show that the derived expressions for the split kinetic fluxes given by Eqs. (39)–(44), together with the flux boundary conditions, lead to valid solutions of the NS equations. For this purpose, compari-

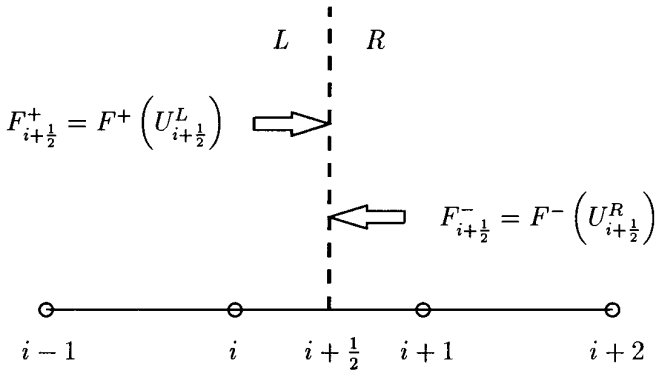

FIG. 4. Definition of symbols used in applying the MUSCL scheme to the KFVS relations for the NS equations.

sons are made with first-order schemes by Steger and Warming [17] and Roe [16], while second-order comparisons are made with the symmetric limited positive second-order (SLIP2) scheme reported by Tatsumi, Martinelli, and Jameson [18]. Central differencing was used in each of these cases to handle the terms introduced by viscous stress and heat flux. A version of the monotone upstream-centered scheme for conservation laws (MUSCL) (van Leer [19]), was used in applying the KFVS relations for the NS equations. The parameters chosen in using MUSCL are defined in the relations

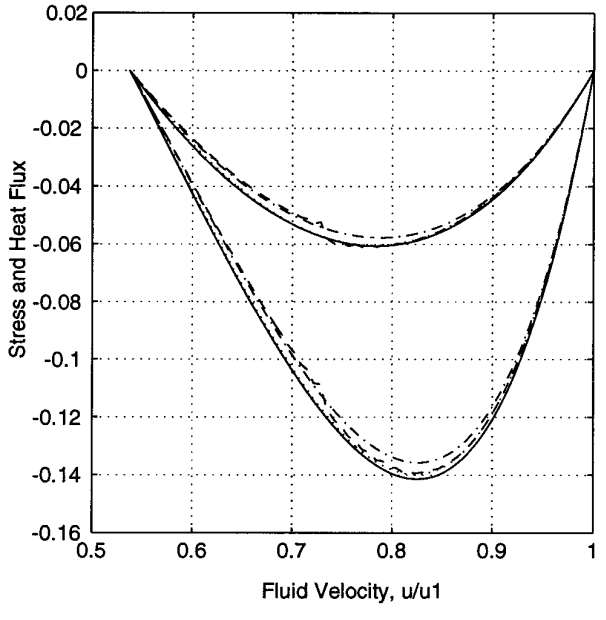

FIG. 5. Normal stress (upper set, $\tau_{nn}/2p$) and heat flux (lower set, q_n/pc) in a shock wave versus the fluid velocity, with the upstream state designated by 1, $M_1 = 1.5$, and $\gamma = 1.4$. The curves were separated by using a factor of 2 in plotting the dimensionless stress. First-order schemes for KFVS, – · – ·, Steger–Warming, – – –, and Roe, · · ·, are compared with the reference solution, ———.

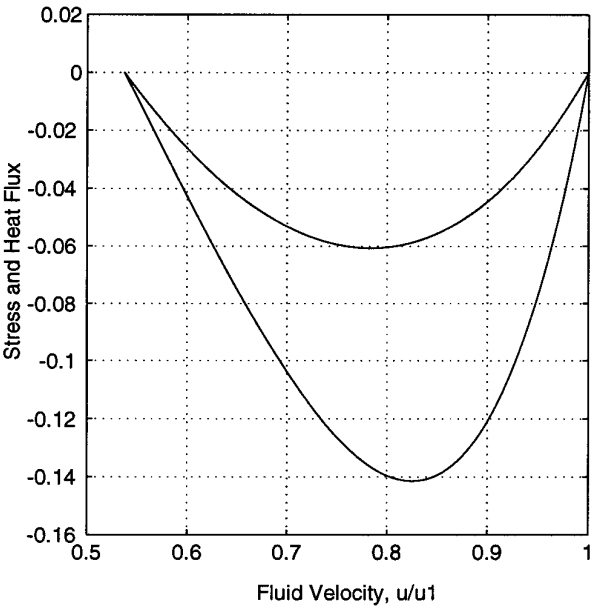

FIG. 6. Normal stress (upper set, $\tau_{nn}/2p$) and heat flux (lower set, q_n/pc) in a shock wave versus the fluid velocity, with the upstream state designated by 1, $M_1 = 1.5$, and $\gamma = 1.4$. The curves were separated by using a factor of 2 in plotting the dimensionless stress. Second-order schemes for KFVS, – · – ·, and Jameson's SLIP2, – – –, are compared with the reference solution, ———.

$$F^{\mathrm{MUSCL}}_{i+1/2} = F^+_{i+1/2} + F^-_{i+1/2}, \tag{69}$$

where

$$F^+_{i+1/2} = F^+(U^{\mathrm{L}}_{i+1/2})$$

$$F^-_{i+1/2} = F^-(U^{\mathrm{R}}_{i+1/2})$$

$$U^{\mathrm{L}}_{i+1/2} = U_i + \frac{\theta_1}{2}\,\mathrm{minmod}[\Delta U_{i-1/2}, \beta\,\Delta U_{i+1/2}]$$

$$U^{\mathrm{R}}_{i+1/2} = U_{i+1} - \frac{\theta_1}{2}\,\mathrm{minmod}[\Delta U_{i+3/2}, \beta\,\Delta U_{i+1/2}]$$

$$\Delta U_{i+1/2} = U_{i+1} - U_i$$

$$\mathrm{minmod}(a,b) \equiv \begin{cases} a & \text{if } |a| \le |b|;\ ab > 0 \\ b & \text{if } |a| > |b|;\ ab > 0 \\ 0 & \text{if } ab < 0 \end{cases}$$

and where the L/R arrangement is defined in Fig. 4. A first-order scheme is obtained for $\theta_1 = 0$ and a second-order scheme for $\theta_1 = 1$. Most of the work was carried out for $\beta = 1.5$. The function $F^+(U^L)$, for example, represents any one of Eqs. (39), (40), (41), or (44). These equations contain spatial derivatives of U as well, and the concept of the function must be generalized to include them.

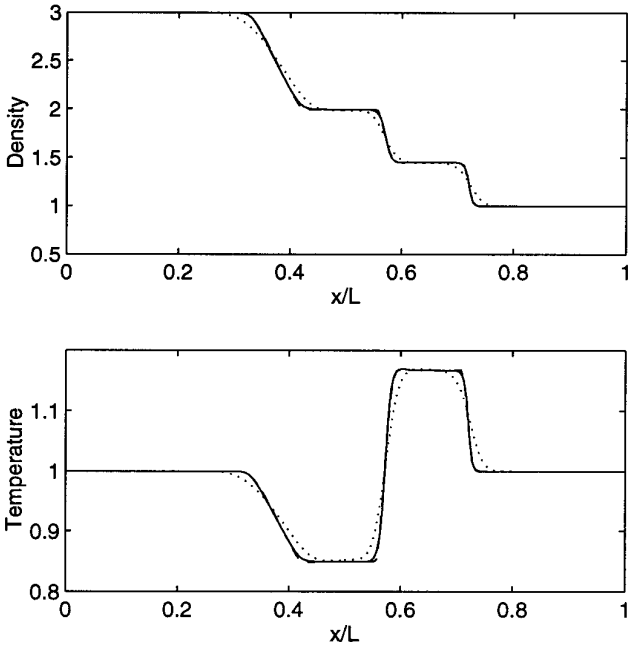

FIG. 7. Shock-tube flow for a pressure ratio of 3, $\gamma = 1.4$, and where the flow is from left to right. Comparisons are for second-order KFVS, ———; Jameson's SLIP2, – – –; and first-order Roe, · · ·. The variables shown are the density $\rho/\rho 1$ and the temperature $T/T1$, where state 1 refers to upstream conditions.

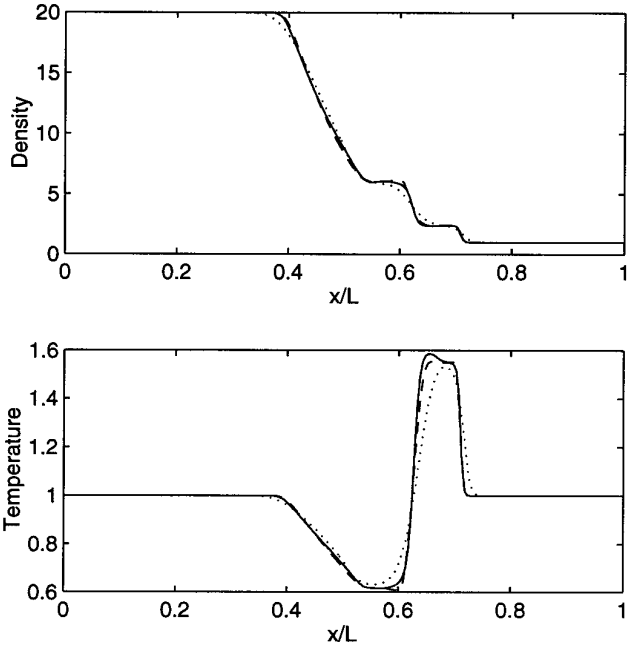

FIG. 8. Shock-tube flow for a pressure ratio of 20, $\gamma = 1.4$, and where the flow is from left to right. Comparisons are for second-order KFVS, ———; Jameson's SLIP2, – – –; and first-order Roe, · · ·. The variables shown are the density $\rho/\rho 1$ and the temperature $T/T1$, where state 1 refers to upstream conditions.

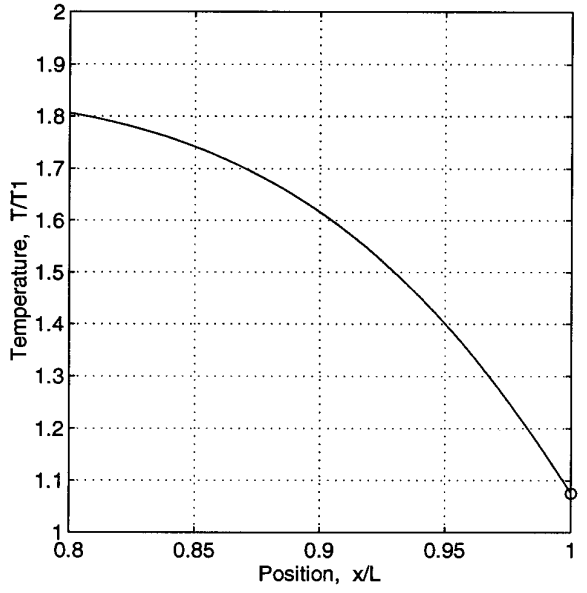

FIG. 9. Temperature ahead of an impulsively started piston in a stationary monatomic gas, where piston Mach number = 1.0 and where use of the flux boundary condition for an isothermal piston leads to a temperature slip at the piston surface (located at $x/L = 1$). Also shown, by the circle symbol, is Patterson's theory [13] for temperature slip in a slightly rarefied monatomic gas.

For a problem with one spatial dimension, the update formula (first-order in time) is then given by

$$U_i^{n+1} = U_i^n - \frac{\Delta t}{\Delta x}(F_{i+1/2}^{\mathrm{MUSCL}} - F_{i-1/2}^{\mathrm{MUSCL}})^n, \qquad (70)$$

where n represents the time step.

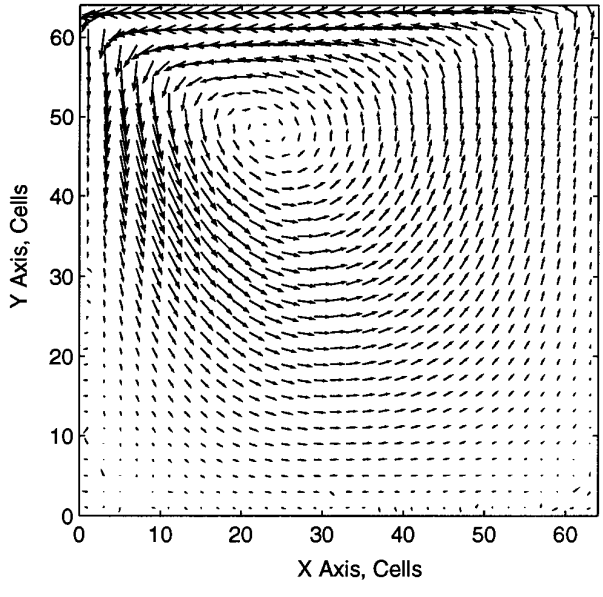

FIG. 10. Velocity field in a square isothermal cavity with a slider plate on top, moving from right to left at a Mach number of 1.0. The gas is assumed to be air and Kn (based on the cavity width) = 0.005.

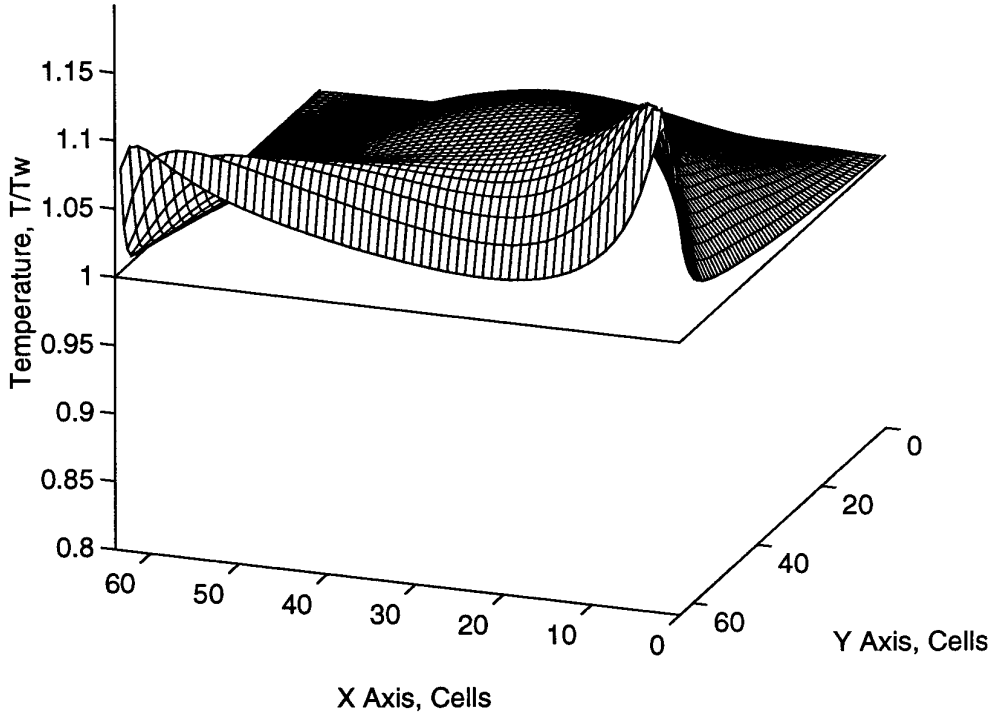

FIG. 11. Temperature distribution in a square isothermal cavity with a slider plate (near face) moving from left to right in view shown; conditions same as in Fig. 10.

The problem of determining the profile for a normal shock wave represents a steady flow for which viscous stress and heat conduction are very important; and this represents an extreme limit that provides appropriate conditions for testing. Although it is well known that the NS equations do not give physically realistic profile predictions for strong shock waves, we are only interested in establishing that valid NS solutions are being obtained. For this purpose, we have the method suggested by von Mises [21] and by Gilbarg and Paolucci [7] for solving the NS equations for steady one-dimensional flow, which can be used as a standard of comparison. To obtain a reliable reference, a four-step Runge–Kutta method and 1200 points in the domain of integration were used. The primary integration takes place in a computational space where the fluid velocity is the independent variable and, because the normal stress and the heat flux variables seem to show the greatest numerical sensitivity, these were selected for display. Figures 5 and 6 give results for a shock-wave Mach number of 1.5 and air as a representative gas. First-order schemes for KFVS, Steger–Warming, and Roe are compared with the reference solution (solid curve) in Fig. 5; it is clear that Roe's scheme compares the best, with Steger–Warming exhibiting the familiar transition near the sonic station and KFVS showing only moderate success. Second-order schemes consisting of KFVS and Jameson's SLIP2, along with the reference solution, are compared in Fig. 6; it is clear that it is not possible to distinguish between them. Higher Mach numbers were also studied and the same general observations were made.

In the same spirit of reviewing extreme conditions, it is appropriate to consider a flow that corresponds to the Euler limit, namely, a shock-tube flow. Because of the presence of the contact surface, it is most useful to display the density and temperature variables as they frequently exhibit large changes there. Figures 7 and 8 present results for pressure ratios (driver to driven gas) of 3 and 20, respectively, and where the flow is from left to right. Starting from the left, the transitions seen are the expansion fan, the contact surface, and the shock wave. We see that there is good agreement between second-order KFVS and SLIP2, with the largest difference at the contact surface, possibly a result of the different limiters used. Roe's first-order scheme clearly shows severe rounding of the profiles. The separation distance between the shock wave and the contact surface grows linearly with time and therefore the relative rounding of the corners would appear to diminish with increasing time. An early time was specifically chosen for display to emphasize the relative difference between the diffrent schemes.

In both the ideal shock-tube and shock-wave problems solid boundaries are absent. However, the case of an impulsively started piston is an example where nonequilibrium effects near a solid boundary can lead to temperature slip.

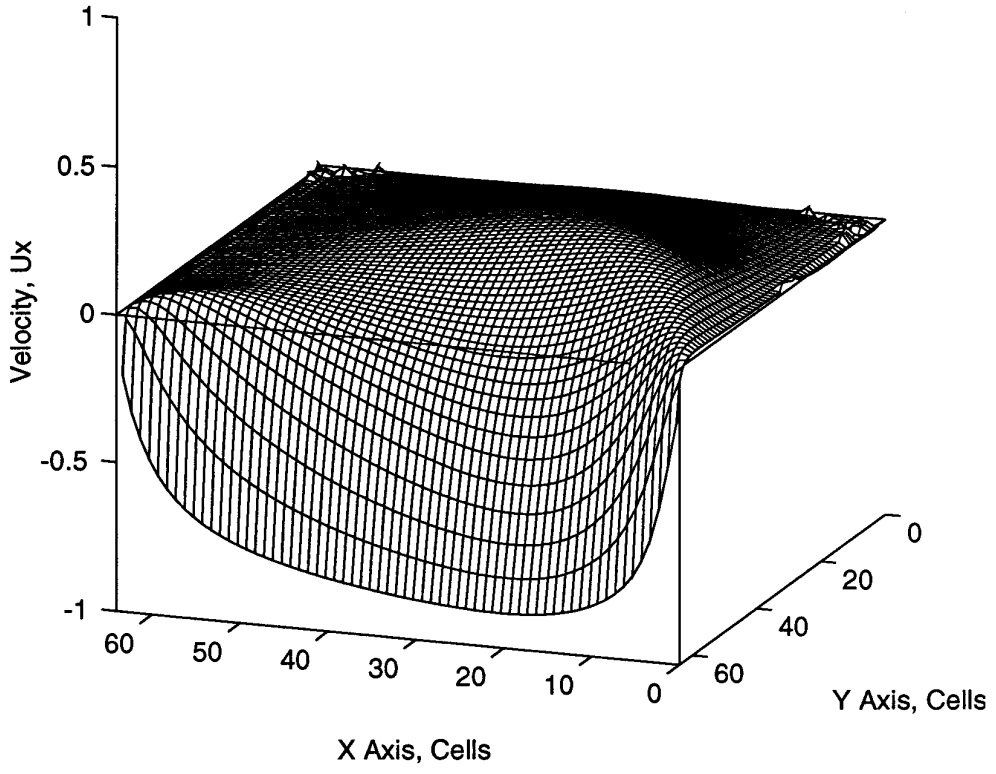

FIG. 12. Velocity component parallel to the slider plate (near face) which is moving from left to right in view shown; conditions same as in Fig. 10 with velocity scaled to the sound speed at the wall temperature.

Figure 9 shows an expanded view of the thermal layer near an isothermal piston, where the piston Mach number is taken to be unity and the gas is ideal and monatomic, and it is clear that the gas temperature near the piston is higher than the piston temperature, as a result of the flux type (DSMC) boundary conditions used in solving the problem. A theoretical expression for temperature slip in a slightly rarefied flow of a monatomic gas was developed by Patterson [13, see Eq. (33), p. 125] and his prediction is shown by the circle symbol. The excellent agreement seen undoubtedly results from the fact that Patterson's theory makes use of the assumptions in NS, and therefore, boundary conditions (62)–(68) used in the numerical solution and the analytical approach used by Patterson correspond closely. A necessary next step, of course, is to carry out comparisons with DSMC simulations to determine the conditions under which the magnitude of the jump is physically correct. This study, which requires careful discussion, will be presented in a follow-on report. The most important observation is that the method introduces slip into the NS formulation in a very natural way through the use of flux boundary conditions.

A final problem to be reviewed is the steady, two-dimensional flow produced by a plate sliding across the open end of a square cavity and for which the temperatures of all four material surfaces are held fixed and equal. This is a well-known problem for which the NS solution, based on the no-slip boundary conditions, leads to singular behavior of the shearing stress, in the two corners defined by the slider plate and the box walls [1]. Because of the shearing motion of the plate, work is done on the fluid, it induces a circulation inside the box, and the fluid is heated as a result of viscous dissipation. However, because of the isothermal walls, heat is conducted out of the gas, and a steady state is reached after a long time has passed. The velocity field shown in Fig. 10 provides an intuitive physical understanding of the flow generated by the sliding plate, which is on top and moves from right to left in the view shown. The computational domain was covered by 64×64 square cells, the plate Mach number was set to 1.0, the Knudsen number (based on the cavity dimension) was set at 0.005, and the gas was assumed to be air at ambient conditions. One of the more interesting results from the solution is the temperature distribution in the box, which is shown in Fig. 11. The dimensionless wall temperature is unity in the figure. If no-slip were present, then the dimensionless gas temperature would also be unity everywhere along the surface, but it can be seen that a significant jump occurs around a great portion of the cavity walls. The same situation develops for the two components of

velocity. Figure 12 displays the velocity component parallel to the slider plate (near face) which is moving left to right in the view shown. If no-slip were present, then the dimensionless gas velocity would be unity (negative) over the length of the plate and zero everywhere else on the box boundary. As can be seen, a significant jump in velocity occurs over the entire plate and, as a result, it appears to suppress the singular behavior of the stress in the two corners. Although the edge-values displayed are actually the values at the midpoints of the cells bordering the walls and one must find the true wall values from extrapolation, the correction is modest and our observations remain unchanged. The small ripples seen in the Fig. 12 are believed to be small vortices that are not fully resolved by the grid used.

VII. CONCLUDING REMARKS

Our work has been guided by the interest in developing a hybrid method using DSMC and NS, where the focus here was limited to a method for handling the NS portion. An Euler scheme introduced by Pullin [15] and further developed by Mandal and Deshpande [12] and by Mallett *et al.* [11], was generalized through use of kinetic-theory concepts to cover the NS equations, and second-order solutions were shown to compare well with established second-order numerical schemes for the NS equations. Because matching must take place in the near-continuum regime, where both DSMC and NS are valid, the NS portion must account for slip at solid boundaries. Use of the kinetic split fluxes was shown to lead to a very natural implementation of DSMC type boundary conditions, and these led to the appearance of slip. Likewise, use of the kinetic split fluxes at an interface between DSMC and NS in a hybrid solution is also expected to be necessary in order to model the correct physics in a nonequilibrium flow, especially when determining the inputs to the DSMC portion. In view of this, the equation set (39)–(44), representing KFVS for the NS equations, is clearly needed in interfacing with DSMC and in applying boundary conditions at a solid surface for the NS portion of a hybrid solution. However, the added step of also using a KFVS scheme for the NS solution itself is not an absolute requirement, as one could argue that any numerical solution of the NS equations would be acceptable, as long as these kinetic split fluxes were used in applying all boundary conditions. Because the DSMC portion is normally expected to take the greater computation time in most problems, one does not need to pick a numerical scheme for the NS portion that minimizes time, and therefore, computation time is not an issue. This allows one to choose a numerical scheme that offers the greatest compatibility with DSMC, which we believe to be the KFVS scheme for the NS equations. On the other hand, in obtaining the data for Figs. 7 and 8, it was found that KFVS and Jameson's SLIP2 required virtually the same computation time. Whether this continues to hold for higher spatial dimensions is unknown.

ACKNOWLEDGMENTS

Many helpful discussions with Tawei Lou and Douglas C. Dahlby concerning their recent DSMC results are gratefully acknowledged. This work was supported in part by NASA under Grant NCC2-5072.

REFERENCES

1. G. K. Batchelor, *An Introduction to Fluid Dynamics* (Cambridge Univ. Press, Cambridge, 1967).
2. G. A. Bird, *Annu. Rev. Fluid Mech.* **10,** 11 (1978).
3. G. A. Bird, *Molecular Gas Dynamics and the Direct Simulation of Gas Flows* (Clarendon Press, Oxford, 1994).
4. J. E. Broadwell, *J. Fluid Mech.* **19,** 401 (1964).
5. S. Chapman and T. G. Cowling, *The Mathematical Theory of Non-Uniform Gases* (Cambridge Univ. Press, Cambridge, 1960).
6. S. Y. Chou, Ph.D. thesis, Stanford University, 1995.
7. D. Gilbarg and D. Paolucci, *J. Rat. Mech. Anal.* **2,** 617 (1953).
8. C. F. Gooch, Ph.D. thesis, Stanford University, 1993.
9. H. Grad, *Commun. Pure Appl. Math.* **2,** 331 (1949).
10. M. N. Macrossan and R. I. Oliver, *Int. J. Num. Meth. Fluids* **17,** 177 (1993).
11. E. R. Mallett, D. I. Pullin, and M. N. Macrossan, *AIAA J.* **33,** No. 9, 1626 (1995).
12. J. C. Mandal and S. M. Deshpande, *Comput. & Fluids* **23,** 447 (1994).
13. G. N. Patterson, *Molecular Flow of Gases* (Wiley, New York, 1956).
14. K. H. Prendergast and K. Xu, *J. Comput. Phys.* **109,** 53 (1993).
15. D. I. Pullin, *J. Comput. Phys.* **34,** 231 (1980).
16. P. L. Roe, *Annu. Rev. Fluid Mech.* **18,** 337 (1986).
17. J. L. Steger and R. F. Warming, *J. Comput. Phys.* **40,** 263 (1981).
18. S. Tatsumi, L. Martinelli, and A. Jameson, *AIAA J.* **33,** No. 2 (1995).
19. B. van Leer, *J. Comput. Phys.* **32,** 101 (1979).
20. W. G. Vincenti and C. H. Kruger, Jr., *Introduction to Physical Gas Dynamics* (Wiley, New York, 1965).
21. R. von Mises, *J. Aero. Sci.* **17,** 551 (1950).
22. L. C. Woods, *An Introduction to the Kinetic Theory of Gases and Magnetoplasmas* (Oxford Univ. Press, Oxford, 1993).